Bulk Fermi Surfaces of the Dirac Type-II Semimetallic Candidates MAl_3 (Where M = V, Nb, and Ta)

K.-W. Chen,[1,2,*] X. Lian,[1,2] Y. Lai,[1,2] N. Aryal,[1,2] Y.-C. Chiu,[1,2] W. Lan,[1,2] D. Graf,[1] E. Manousakis,[1,2] R. E. Baumbach,[1,2] and L. Balicas[1,2,†]

[1]*National High Magnetic Field Laboratory, Florida State University, Tallahassee, Florida 32310, USA*
[2]*Department of Physics, Florida State University, Tallahassee, Florida 32306, USA*

(Received 6 March 2018; published 15 May 2018)

We report a de Haas–van Alphen (dHvA) effect study on the Dirac type-II semimetallic candidates MAl_3 (where, M = V, Nb and Ta). The angular dependence of their Fermi surface (FS) cross-sectional areas reveals a remarkably good agreement with our first-principles calculations. Therefore, dHvA supports the existence of tilted Dirac cones with Dirac type-II nodes located at 100, 230 and 250 meV above the Fermi level ε_F for VAl_3, $NbAl_3$ and $TaAl_3$ respectively, in agreement with the prediction of broken Lorentz invariance in these compounds. However, for all three compounds we find that the cyclotron orbits on their FSs, including an orbit nearly enclosing the Dirac type-II node, yield trivial Berry phases. We explain this *via* an analysis of the Berry phase where the position of this orbit, relative to the Dirac node, is adjusted within the error implied by the small disagreement between our calculations and the experiments. We suggest that a very small amount of doping could displace ε_F to produce topologically nontrivial orbits encircling their Dirac node(s).

DOI: 10.1103/PhysRevLett.120.206401

Condensed-matter systems provide accessible platforms for the discovery of quasiparticles with properties akin to particles predicted by high-energy physics. Dirac type-I compounds, such as Cd_3As_2 [1,2] or Na_3Bi, [3,4]), and Weyl type-I systems, like (Ta,Nb)(P,As) [5–7], were recently discovered and are garnering a lot of attention. According to Ref. [8], solid state systems would even offer the potential of finding fermionic excitations that have no analog in high-energy physics, such as three-component fermions [9]. Very recently, so-called type-II Dirac-Weyl semimetals, which violate Lorentz-symmetry, were discovered and are being intensively studied. In type-II Dirac-Weyl semimetals, the crossings between energy bands remain protected, but the spectra of the Dirac-Weyl cones are strongly tilted due to an additional momentum dependent term; thus, they break the Lorentz invariance. These Dirac-Weyl type-II nodes become singular points connecting electron and hole pockets in the spectral function. The associated quasiparticles can be observed in condensed matter systems, but the analog particles are absent in Lorentz invariant high energy physics. Type-II Dirac-Weyl semimetallic systems were proposed to display unique properties, such as Klein tunneling in momentum space [10], orientation-dependent chiral anomaly [11], and a modified anomalous Hall conductivity [12].

A number of Weyl type-II semimetals were already experimentally studied, including $MoTe_2$ [13–15], WTe_2 [16–18], Ta_3S_2 [19], LaAlGe [20], and $TaIrTe_4$ [21,22]. And although several Dirac type-II compounds were also reported, e.g., VAl_3 [23,24], YPd_2Sn [25], KMgBi [26], and $(Pt, Pd)Te_2$ [27–29], only the last two compounds were studied experimentally via angle-resolved photoemission spectroscopy (ARPES) and quantum oscillatory phenomena [27,28,30]. Therefore, Dirac type-II systems remain to be unambiguously identified and characterized experimentally. For instance, and in addition to the aforementioned predictions, Dirac type-II semimetals have been predicted to become Weyl type-II systems or topological crystalline insulators when time reversal or inversion symmetries are broken [23,24]. However, exposing the unique transport properties of such compounds is a difficult task due to the distance of the Dirac type-II nodes with respect to the Fermi level, which, in addition, is crossed by topologically trivial and nontrivial bands.

Here, we report the synthesis of the chemical analogues $(V, Nb, Ta)Al_3$ that were predicted to display Dirac type-II nodes [23]. The topography of their Fermi surfaces, revealed through the de Haas–van Alphen (dHvA) effect, are found to display remarkably good agreement with band structure calculations. Therefore, our experimental study indicates that these compounds would break Lorentz invariance [23]. The Dirac type-II nodes in VAl_3 and $NbAl_3$ are found to be relatively close to Fermi level, i.e., at respectively $\approx$100 meV and $\approx$230 meV above it, making these compounds promising candidates for tuning the Fermi level (e.g., via chemical substitution) to displace electronic orbits towards the location of the Dirac node. In fact, we find that one of the observed cyclotron orbits nearly encloses the Dirac type-II node(s), and although it yields a topologically trivial Berry-phase, a small amount

of doping or displacement of ε_F could lead to a topologically nontrivial orbit.

Details concerning single-crystal growth can be found in the Supplemental Material (SM) file [31]. Supplemental Figs. S1, S2, S3, and S4 provide x-ray diffraction, resistivity, a discussion on the role of Al inclusions [32], and values for the extracted mobilities, respectively [31]. Density functional theory calculations were performed with the Wien2K [33] implementation of density functional theory (DFT) with the Perdew-Burke-Ernzerhof parametrization of the generalized gradient approximation (GGA-PBE) [34]. The angular dependency of the Fermi-surface cross sectional areas were computed through SKEAF [35]. The validity of these results were verified through the Quantum EXPRESSO implementation of DFT obtaining very similar results [36,37].

Here, we report a study on the electronic structure at the Fermi level of the $M\mathrm{Al}_3$ family through the dHvA-effect superimposed onto torque magnetometry. The $M\mathrm{Al}_3$ compounds crystalize in a body-centered tetragonal Bravais lattice belonging to the space group $I4/mmm$ (No. 139) as shown in Fig. 1(a). Lattice constants determined through x-ray diffraction are given in the SM [31]. According to DFT, there are two tilted Dirac cones along the $Z-\Gamma-Z$ line within the first Brillouin zone [see Fig. 1(c)], with the Dirac node located at the touching point between the electron and hole cones. As seen through Figs. 1(c) to 1(e), the crossing of the hole bands with the Fermi level produces two holelike Fermi surface sheets, i.e., the α and the β orbits, while the electron bands lead to the γ pockets. The proximity of the β and γ orbits to the Dirac type-II nodes would make them prime candidates for carriers displaying nontrivial Berry phases. In contrast, we would expect the α pocket along the Σ_1-Z line, which is absent in NbAl_3, to yield topologically trivial orbits. As we show below, the electron pocket displays a "helixlike" shape, while the hole one yields a "dumbbell-like" sheet that supports two orbits: the neck (or the β_1 orbit) and the belly (or the β_2 orbit).

The torque signal $\tau(\mu_0 H)$ can be expressed in terms of the component of the magnetization perpendicular to the external field $\mu_0 H$: $M_\perp = \tau/V\mu_0 H$, where V is the volume of the sample. From the Onsager relation, the frequencies F of the oscillatory signal are proportional to the extremal cross sectional areas A of a given Fermi surface sheet:

$$F = \frac{\hbar}{2\pi e} A, \tag{1}$$

where $\hbar$ is the reduced Planck constant and e is the electrical charge. Figures 2(a), 2(c), and 2(e) display $M_\perp$ as a function of $\mu_0 H$, collected at a temperature $T = 0.4$ K, for the V, Nb, and Ta compounds, respectively, where a superimposed oscillatory signal, or the dHvA effect, can be observed. These traces were collected at an angle $\theta = 22°$ (for the V compound), 24° (Nb), and 30° (Ta), respectively, where $\theta = 0°$ and 90° correspond to fields along the c and the a axes, respectively. The anomaly observed in TaAl_3, near $\mu_0 H \simeq 20$ T, is most likely an indication for the quantum limit associated to the α orbit. Figures 2(b), 2(d), and 2(f), display the temperature dependence of the main peaks or frequencies observed in the FFT spectra extracted from the oscillatory signal plotted as a function of inverse field $(\mu_0 H)^{-1}$ for each compound (see insets). The dHvA signals were obtained after fitting the background of $M_\perp$ to

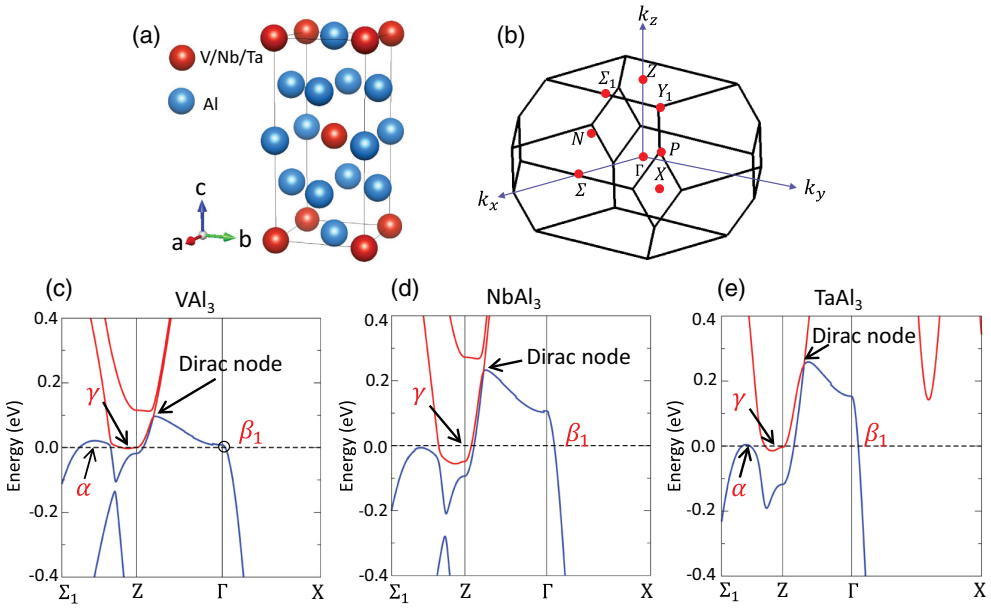

FIG. 1. (a) Crystal structure of the $M\mathrm{Al}_3$ family. Red spheres represents V, Nb, or T, while the blue ones depict Al atoms. (b) Brillouin zone and high symmetry points. (c),(d),(e) The calculated band structures for all three compounds. Dirac type-II nodes along the $Z-\Gamma$ lines, and the Fermi surface cross sectional areas associated with the α, β_1, and γ dHvA orbits are indicated by arrows.

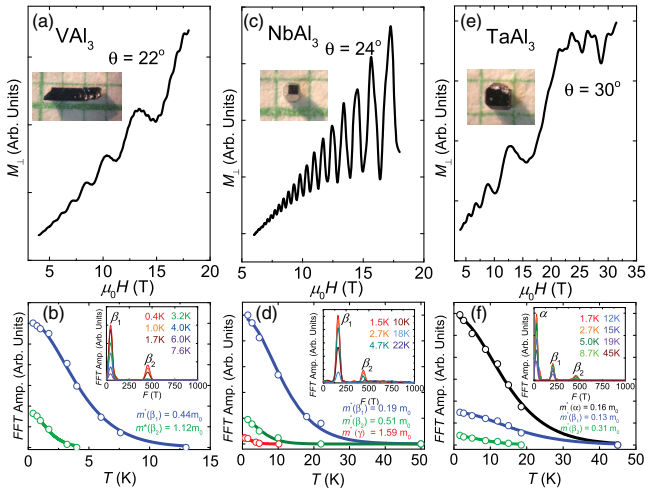

FIG. 2. Transverse component of the magnetization $M_\perp$ as a function of magnetic field $\mu_0 H$ for (a) VAl_3, (c) $NbAl_3$, and (e) $TaAl_3$, respectively. These traces were collected at angles $\theta = 22°$, 24°, and 30°, respectively, between the external field and the c axis. These traces were measured at a temperature $T = 0.4$ K. (b),(d),(f) Amplitude of the main peaks observed in the Fourier spectra of the oscillatory signal extracted from each compound as a function of the temperature. Insets: Fast Fourier transforms of the dHvA signal extracted from each compound at several temperatures.

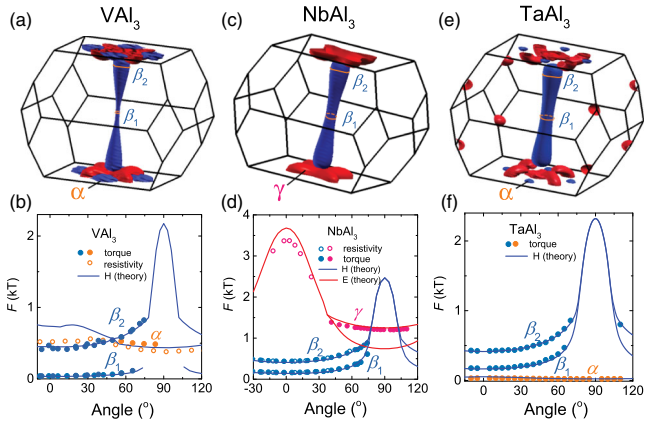

FIG. 3. Fermi surfaces for (a) VAl_3, (c) $NbAl_3$, (e) $TaAl_3$, respectively. Hole- and electronlike pockets are depicted in blue and in red, respectively. β_1 and β_2 orbits match the frequencies calculated for the "neck" and the "belly" cross sectional areas of the dumbbell like pockets. The α orbit can be associated to a holelike ellipsoid of topologically trivial character. The γ orbit can be associated with the large "helix" like electron pocket. (b),(d), (f) Cyclotron frequencies F as functions of the angle θ relative to crystallographic c axis. Open and closed symbols depict SdH and dHvA data, respectively. Solid lines depict the angular dependence of the FS extremal cross sectional areas predicted theoretically.

a polynomial and its subsequent subtraction. By fitting the amplitude of the FFT peaks as a function of the temperature to the thermal damping term in the Lifshitz-Kosevich formalism [38] [see Eq. (2)], one can extract the carrier effective masses m^*, see Figs. 2(b), 2(d), and 2(f). For the neck $F_{\beta_1} = 35$ T and belly $F_{\beta_2} = 410$ T orbits on the "dumbbell" hole pocket of VAl_3, we extracted $m^*_{\beta_1} = 0.44\ m_0$ and $m^*_{\beta_2} = 1.12\ m_0$, respectively. Here, m_0 is the free-electron mass. As we show below, these orbits were identified after a detailed comparison with the DFT calculations. For $NbAl_3$, we extracted $F_{\beta_1} = 163$ T with $m^*_{\beta_1} = 0.19\ m_0$ and $F_{\beta_2} = 440$ T with corresponding $m^*_{\beta_2} = 0.51\ m_0$. For $TaAl_3$, we identified $F_{\beta_1} = 174$ T with $m^*_{\beta_1} = 0.13\ m_0$ and $F_{\beta_2} = 423$ T with $m^*_{\beta_2} = 0.31\ m_0$. We are also able to detect the large electron γ pocket of $NbAl_3$ through magnetoresistivity or Shubnikov–de Haas (SdH) measurements under fields up to $\mu_0 H = 31$ T, yielding $F_\gamma \simeq 3300$ T with $m^*_\gamma = 1.59\ m_0$. These m^* values are not particularly light, which indicates that these orbits are not very close to the linearly dispersive region of the bands.

In order to study the geometry of the Fermi surface, we measured the angular dependence of the dHvA oscillations. A comparison between the DFT calculations and the angular dependence of the dHvA frequencies, shown in Figs. 3(a) to 3(f), indicates that the β_1 and β_2 orbits of the MAl_3 compounds correspond to the minimum and maximum cross sectional areas of the "dumbbell" hole pockets (in blue, around the Γ-points). In Figures 3(b), 3(d), and 3(f), markers correspond to the experimental points, while lines depict the angular dependence of the FS cross sectional areas according to DFT. The topologically trivial α orbit corresponds to ellipsoids (in blue) extending along the $Z - \Sigma_1$ lines in VAl_3 and in $TaAl_3$, which are absent in $NbAl_3$. Finally, the γ orbit corresponds to the electronlike "helix" sheet, depicted in red around the Z point. As seen through Figs. 3(b), 3(d), and 3(f), the experimentally obtained values for the β_1 and β_2 orbits agree very well with the calculated ones, but they become unmeasurable for $\theta > 75°$. This suggests either very anisotropic effective masses or, most likely, anisotropic scattering rates. The α orbit follows the theoretical predictions with some deviations that can be partially attributed to sample misalignment. As for the γ orbit, it was observable only in $NbAl_3$; hence, we chose not to plot the respective theoretical traces for VAl_3 and $TaAl_3$ in Figs. 3(b) and 3(f). Its nonobservation is likely the result of large cross sectional areas (or frequencies) combined with heavier effective masses leading to low mobilities. The very good agreement between the experimentally determined and the calculated FS cross sectional areas supports the existence of a Dirac Type-II node located at ≃100, ≃230, and 250 meV above the Fermi level in VAl_3, $NbAl_3$, and $TaAl_3$, respectively. Notice that, our calculations do not yield the same FS topography as the ones reported in Refs. [23,24]. For instance, in their calculations, the dumbbell-like hole pocket would have a quite different geometry. The exact position of the Dirac nodes relative to ε_F also differs between our calculations and those in Refs. [23,24].

Now, we address the topological character of the observed orbits; the Lifshitz-Kosevich formalism describing the field and the temperature-dependence of the dHvA oscillations is given by [38]:

$$M_{\parallel} = -AB^{1/2}R_T R_D R_S \sin\left[2\pi\left(\frac{F}{B} - \gamma + \delta\right)\right], \quad (2)$$

where $\gamma = 1/2$ for a parabolic band and $= 0$ for a linear one. The phase shift δ is determined by the dimensionality of the Fermi surface taking values $\delta = \pm 1/8$ for minima and maxima cross sectional areas of a three-dimensional Fermi surface, respectively. $R_T = X/\sinh(X)$ is the thermal damping factor, where $X = 2\pi^2 k_B m^* T/e\hbar B$, $R_D = \exp(-2\pi^2 k_B m^* T_D/e\hbar B)$ is the Dingle damping factor, where m^* is the effective mass and $T_D = \hbar/2\pi k_B \tau_q$ from which one can evaluate the quasiparticle lifetime τ_q. $R_s = \cos(\pi g m^*/2m_0)$ is the spin damping factor, where g is the Landè g factor. In order to extract the correct phase of the dHvA oscillations, we make use of the magnetic susceptibility $\Delta\chi = d(\Delta M)/d(\mu_0 H)$:

$$\Delta\chi \sim \mathrm{sign} R_S \cos\left[2\pi\left(\frac{F}{B} - \gamma + \delta\right)\right], \quad (3)$$

the phase of the oscillations is given by $\phi = -(\gamma - \delta)$, where $\gamma = (1/2 - \phi_B/2\pi)$, with ϕ_B being the Berry phase, and $\delta = 0$ or $\pm 1/8$ for two- and three-dimensional (3D) FSs, respectively. For trivial 3D bands, $\phi_B = 0$; hence, one expects $\phi = 1/2 \mp 1/8 = 3/8$ or $5/8$, for maximum and minimum cross sectional areas, respectively. Notice that, the value of ϕ can be affected by the sign of the spin damping factor R_S, and this has to be carefully considered when extracting the Berry phase. To experimentally extract the phase, we assign integer Landau level indices n to the peaks in $\Delta\chi$ (maxima in the density of states [39]) and $n + 1/2$ to the valleys. The phase ϕ can be extracted from the intercept of the extrapolation of n as function of $(\mu_0 H)^{-1}$; Landau fan diagrams are shown in Figs. 4(a), 4(b), and 4(c), for VAl_3, $NbAl_3$, and $TaAl_3$, respectively. For all of the three compounds, we obtain $\phi \sim +1/8$ for the β_1 orbit that encircles the Γ-point in the FBZ which, according to DFT, corresponds to a minimal cross sectional area of a trivial parabolic band. Hence, this anomalous $1/8$ value can be understood as $-1/2 + 5/8$, where the $-1/2$ term is attributable to a "minus" sign provided by the spin dephasing term R_s. The β_2 orbit is the one encircling the Dirac node. However, it is difficult to extract ϕ for the β_2 orbit of both the VAl_3 and $TaAl_3$ compounds given that their higher frequencies are superimposed onto those of the α and β_1 orbits. Fortunately, we were able to extract $\phi \sim 3/8$ for the β_2 orbit of $NbAl_3$ through torque measurements. As for the α orbit associated with the trivial parabolic band of $TaAl_3$, we find $\phi \simeq 0.44 \gtrsim 3/8$, see Fig. 4(c). This value was confirmed by superconducting quantum interference device (SQUID) magnetometry measurements. See Supplemental Figs. S5, S6, S7, and S8 for band pass filter and phase analysis of the dHvA signal, Berry-phase analysis based on resistivity, based on SQUID magnetometry, and the analysis of the spin dephasing term for VAl_3, $NbAl_3$, and $TaAl_3$, respectively [31]. In the same Ref. [31], we provide a calculation of the Berry-phase based upon the model of Ref. [23]. We show that within the error implied by very small displacements in ε_F introduced into the DFT calculations to match the experimental results, the β_2 orbit could not enclose the Dirac node(s) yielding a Berry phase $< \pi/2$.

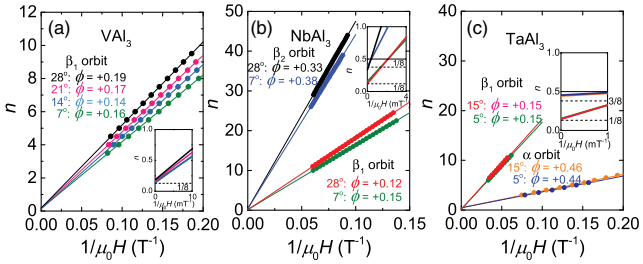

FIG. 4. (a),(b),(c) Landau level index n as a function of $(\mu_0 H)^{-1}$ for all three compounds and for several angles θ between the external field and the c axis. Here, the n indices were assigned to the peaks in the longitudinal resistivity $\Delta\rho_{xx}$ or in the magnetic susceptibility $\Delta\chi$ while $n + 1/2$ were assigned to the minima. The intercept yields the phase ϕ_B, which acquires values of $\sim 1/8$ for the β_1 orbit and of $\sim 3/8$ for the α and β_2 orbits.

In summary, we unveiled the Fermi surfaces of the MAl_3 family through quantum oscillations measurements combined with band structure calculations. Among all three compounds, VAl_3 displays the closest Dirac type-II node with respect to its Fermi level (~100 meV). The extracted Berry phases for all of the measured Fermi surfaces are consistent with time-reversal-symmetric systems displaying discrete and topologically trivial values. Although one of the orbits of $NbAl_3$ nearly encloses the Dirac node, it also leads to the observation of a trivial Berry-phase because it is not located in the same k_z plane as the Dirac type-II point. The situation here is somewhat akin to the one discussed in Ref. [39], where the Berry phase quickly becomes trivial as the Fermi level is displaced away from the Dirac node(s), or as the dispersion crosses over from linear to quadratic. Notice that, our calculations indicate that the Dirac node can be displaced towards the Fermi level as the ionic size of the transition metal decreases, indicating a role for chemical substitution. One would need only a small displacement of the Fermi level of the order of 10 meV to stabilize a topologically nontrivial orbit enclosing the Dirac node. Notice that, this approach might also contribute to stabilize bulk superconductivity [40] or a Weyl type-II state if one chose magnetic dopants [23].

The data in this manuscript is available through a request to the corresponding authors.

The authors thank H.-Z. Lu at South University of Science and Technology of China for informative discussions and M. Khan at Louisiana State University for help with our measurements. This work was supported by DOE-BES

through Award No. DE-SC0002613. K. W. C. was partially supported by the NHMFL-UCGP program. The NHMFL is supported by NSF through NSF-DMR-1157490 and the State of Florida.

*Corresponding author.
kchen@magnet.fsu.edu
†Corresponding author.
balicas@magnet.fsu.edu

[1] Z. K. Liu, J. Jiang, B. Zhou, Z. J. Wang, Y. Zhang, H. M. Weng, D. Prabhakaran, S.-K. Mo, H. Peng, P. Dudin, T. Kim, M. Hoesch, Z. Fang, X. Dai, Z. X. Shen, D. L. Feng, Z. Hussain, and Y. L. Chen, Nat. Mater. **13**, 677 (2014).
[2] Z. Wang, H. Weng, Q. Wu, X. Dai, and Z. Fang, Phys. Rev. B **88**, 125427 (2013).
[3] Z. Wang, Y. Sun, X.-Q.Chen, C. Franchini, G. Xu, H. Weng, X. Dai, and Z. Fang, Phys. Rev. B **85**, 195320 (2012).
[4] Z. K. Liu, B. Zhou, Y. Zhang, Z. J. Wang, H. M. Weng, D. Prabhakaran, S.-K. Mo, Z. X. Shen, Z. Fang, X. Dai, Z. Hussain, and Y. L. Chen, Science **343**, 864 (2014).
[5] H. Weng, C. Fang, Z. Fang, B. A. Bernevig, and X. Dai, Phys. Rev. X **5**, 011029 (2015).
[6] B. Q. Lv, H. M. Weng, B. B. Fu, X. P. Wang, H. Miao, J. Ma, P. Richard, X. C. Huang, L. X. Zhao, G. F. Chen, Z. Fang, X. Dai, T. Qian, and H. Ding, Phys. Rev. X **5**, 031013 (2015).
[7] S.-Y. Xu *et al.*, Sci. Adv. **1**, e1501092 (2015).
[8] B. Bradlyn, J. Cano, Z. Wang, M. G. Vergniory, C. Felser, R. J. Cava, and B. A. Bernevig, Science **353**, aaf5037 (2016).
[9] B. Q. Lv, Z.-L. Feng, Q.-N. Xu, X. Gao, J.-Z. Ma, L.-Y. Kong, P. Richard, Y.-B. Huang, V. N. Strocov, C. Fang, H.-M. Weng, Y.-G. Shi, T. Qian, and H. Ding, Nature (London) **546**, 627 (2017).
[10] T. E. O'Brien, M. Diez, and C. W. J. Beenakker, Phys. Rev. Lett. **116**, 236401 (2016).
[11] M. Udagawa and E. J. Bergholtz, Phys. Rev. Lett. **117**, 086401 (2016).
[12] A. A. Zyuzin and R. P. Tiwari, JETP Lett. **103**, 717 (2016).
[13] K. Deng, G. Wan, P. Deng, K. Zhang, S. Ding, E. Wang, M. Yan, H. Huang, H. Zhang, Z. Xu, J. Denlinger, A. Fedorov, H. Yang, W. Duan, H. Yao, Y. Wu, S. Fan, H. Zhang, X. Chen, and S. Zhou, Nat. Phys. **12**, 1105 (2016).
[14] L. Huang, T. M. McCormick, M. Ochi, Z. Zhao, M.-T. Suzuki, R. Arita, Y. Wu, D. Mou, H. Cao, J. Yan, N. Trivedi, and A. Kaminski, Nat. Mater. **15**, 1155 (2016).
[15] Z. Wang, D. Gresch, A. A. Soluyanov, W. Xie, S. Kushwaha, X. Dai, M. Troyer, R. J. Cava, and B. A. Bernevig, Phys. Rev. Lett. **117**, 056805 (2016).
[16] F. Y. Bruno, A. Tamai, Q. S. Wu, I. Cucchi, C. Barreteau, A. de la Torre, S. McKeown Walker, S. Riccò, Z. Wang, T. K. Kim, M. Hoesch, M. Shi, N. C. Plumb, E. Giannini, A. A. Soluyanov, and F. Baumberger, Phys. Rev. B **94**, 121112(R) (2016).
[17] H. Huang, S. Zhou, and W. Duan, Phys. Rev. B **94**, 121117 (2016).
[18] C. Wang *et al.*, Phys. Rev. B **94**, 241119(R) (2016).
[19] G. Chang, S.-Y. Xu, D. S. Sanchez, S.-M. Huang, C.-C. Lee, T.-R. Chang, G. Bian, H. Zheng, I. Belopolski, N. Alidoust, H.-T. Jeng, A. Bansil, H. Lin, and M. Z. Hasan, Sci. Adv. **2**, e1600295 (2016).
[20] S.-Y. Xu *et al.*, Sci. Adv. **3**, e1603266 (2017).
[21] K. Koepernik, D. Kasinathan, D. V. Efremov, S. Khim, S. Borisenko, B. Büchner, and J. van den Brink, Phys. Rev. B **93**, 201101(R) (2016).
[22] S. Khim, K. Koepernik, D. V. Efremov, J. Klotz, T. Förster, J. Wosnitza, M. I. Sturza, S. Wurmehl, C. Hess, J. van den Brink, and B. Büchner, Phys. Rev. B **94**, 165145 (2016).
[23] T.-R. Chang, S.-Y. Xu, D. S. Sanchez, W.-F. Tsai, S.-M. Huang, G. Chang, C.-H. Hsu, G. Bian, I. Belopolski, Z.-M. Yu, S. A. Yang, T. Neupert, H.-T. Jeng, H. Lin, and M. Z. Hasan, Phys. Rev. Lett. **119**, 026404 (2017).
[24] Y. Ge, W. Wan, Y. Liu, and Y. Zhang, J. Phys. Condens. Matter **29**, 415701 (2017).
[25] P.-J. Guo, H.-C. Yang, K. Liu, and Z.-Y. Lu, Phys. Rev. B **95**, 155112 (2017).
[26] C. Le, S. Qin, X. Wu, X. Dai, P. Fu, C. Fang, and J. Hu, Phys. Rev. B **96**, 115121 (2017).
[27] M. Yan, H. Huang, K. Zhang, E. Wang, W. Yao, K. Deng, G. Wan, H. Zhang, M. Arita, H. Yang, Z. Sun, H. Yao, Y. Wu, S. Fan, W. Duan, and S. Zhou, Nat. Commun. **8**, 257 (2017).
[28] H.-J. Noh, J. Jeong, E.-J. Cho, K. Kim, B. I. Min, and B.-G. Park, Phys. Rev. Lett. **119**, 016401 (2017).
[29] K. Zhang, M. Yan, H. Zhang, H. Huang, M. Arita, Z. Sun, W. Duan, Y. Wu, and S. Zhou, Phys. Rev. B **96**, 125102 (2017).
[30] F. Fei, X. Bo, R. Wang, B. Wu, J. Jiang, D. Fu, M. Gao, H. Zheng, Y. Chen, X. Wang, H. Bu, F. Song, X. Wan, B. Wang, and G. Wang, Phys. Rev. B **96**, 041201(R) (2017).
[31] See Supplemental Material at http://link.aps.org/supplemental/10.1103/PhysRevLett.120.206401 for Powder X-ray diffraction pattern from $M\mathrm{Al}_3$ single crystals, Electrical resistivity as a function of the temperature for VAl_3, dHvA oscillations of VAl_3 single-crystals containing Al inclusions, Dingle plots for all three $M\mathrm{Al}_3$ compounds, Analysis of the quantum oscillations using band pass filters, Berry phase analysis for NbAl_3 based on the longitudinal magnetoresistivity ρ_{xx}, Landau fan plots for VAl_3 and TaAl_3 from SQUID magnetometry data, Spin reduction factors R_S and Landé g-factors, DFT bands at two slightly different k_z planes, Plots of the Berry connection vector.
[32] G. Li, Z. Xiang, F. Yu, T. Asaba, B. Lawson, P. Cai, C. Tinsman, A. Berkley, S. Wolgast, Y. S. Eo, D.-J. Kim, C. Kurdak, J. W. Allen, K. Sun, X. H. Chen, Y. Y. Wang, Z. Fisk, and L. Li, Science **346**, 1208 (2014).
[33] K. Schwarz, P. Blaha, and G. Madsen, Comput. Phys. Commun. **147**, 71 (2002).
[34] J. P. Perdew, K. Burke, and M. Ernzerhof, Phys. Rev. Lett. **77**, 3865 (1996).
[35] P. M. C. Rourke and S. R. Julian, Comput. Phys. Commun. **183**, 324 (2012).
[36] P. Giannozzi *et al.*, J. Phys. Condens. Matter **21**, 395502 (2009).

[37] P. Giannozzi *et al.*, J. Phys. Condens. Matter **29**, 465901 (2017).
[38] D. Shoenberg, *Magnetic Oscillations in Metals* (Cambridge University Press, Cambridge, 2011).
[39] C. M. Wang, H.-Z. Lu, and S.-Q. Shen, Phys. Rev. Lett. **117**, 077201 (2016).
[40] E. Leyarovski, L. Leyarovska, E. Krasnopyorov, L. Kokot, R. Horyń, and T. Mydlarz, Z. Phys. B **27**, 57 (1977).